The interplay between electron transport chain function and iron regulatory factors influences melanin formation in *Cryptococcus neoformans*

Peng Xue [a,b,] , Eddy Sánchez-León [a,#], Guanggan Hu [a], Christopher WJ Lee [a], Braydon Black [a], Anna Brisland [a], Haohua Li [a], Won Hee Jung[c], James W. Kronstad[a#]

[a]Michael Smith Laboratories, Department of Microbiology and Immunology, University of British Columbia, Vancouver, British Columbia, Canada

[c]Department of Systems Biotechnology, Chung-Ang University, Anseong, Republic of Korea

[b]Present address: Nantong Key Laboratory of Environmental Toxicology, Department of Occupational Medicine and Environmental Toxicology, School of Public Health, Nantong University, Nantong, Jiangsu, China

Running Title: Electron transport chain regulation of melanin

[#]Address correspondence to James W. Kronstad, kronstad@msl.ubc.ca.

[#]Peng Xue and Eddy Sánchez-León contributed equally to this work. Author order was based on initiation of the project by Peng Xue.

KEYWORDS electron transport chain, reactive oxygen species, iron regulation, fungal pathogenesis, melanin formation, RNA-Seq

ABSTRACT

Mitochondrial functions are critical for the ability of the fungal pathogen *Cryptococcus neoformans* to cause disease. However, mechanistic connections between key functions such as the mitochondrial electron transport chain (ETC) and virulence factor elaboration have yet to be thoroughly characterized. Here, we observed that inhibition of ETC complex III suppressed melanin formation, a major virulence factor. This

inhibition was partially blocked upon loss of Cir1 or HapX, two transcription factors that regulate iron acquisition and use. In this regard, loss of Cir1 derepresses the expression of laccase genes as a potential mechanism to restore melanin, while HapX may condition melanin formation by controlling oxidative stress. We hypothesize that ETC dysfunction alters redox homeostasis to influence melanin formation. Consistent with this idea, inhibition of growth by hydrogen peroxide was exacerbated in the presence of the melanin substrate L-DOPA. Additionally, loss of the mitochondrial chaperone Mrj1, which influences the activity of ETC complex III and reduces ROS accumulation, also partially blocked antimycin A inhibition of melanin. The phenotypic impact of mitochondrial dysfunction was consistent with RNA-Seq analyses of WT cells treated with antimycin A or L-DOPA, or cells lacking Cir1 that revealed influences on transcripts encoding mitochondrial functions (e.g., ETC components and proteins for Fe-S cluster assembly). Overall, these findings reveal mitochondria-nuclear communication via ROS and iron regulators to control virulence factor production in *C. neoformans*.

IMPORTANCE

There is a growing appreciation of the importance of mitochondrial functions and iron homeostasis in the ability of fungal pathogens to sense the vertebrate host environment and cause disease. Many mitochondrial functions such as heme and iron-sulfur cluster biosynthesis, and the electron transport chain (ETC), are dependent on iron. Connections between factors that regulate iron homeostasis and mitochondrial activities are known in model yeasts and are emerging for fungal pathogens. In this study, we identified connections between iron regulatory transcription factors (e.g., Cir1 and HapX) and the activity of complex III of the ETC that influence the formation of melanin, a key virulence factor in the pathogenic fungus *Cryptococcus neoformans*. This fungus causes meningoencephalitis in immunocompromised people and is a major threat to the HIV/AIDS population. Thus, understanding how mitochondrial functions influence virulence may support new therapeutic approaches to combat diseases caused by *C. neoformans* and other fungi.

63 **INTRODUCTION**

64 Mitochondria play a central role in respiratory metabolism for fungal pathogens
65 of plants and animals, and support the ability of fungi to sense environmental and host
66 conditions (1-5). The importance of mitochondrial functions in pathogenesis has been
67 demonstrated for a number of fungal pathogens of humans including *Cryptococcus*
68 *neoformans* and the related species *C. gattii* (1, 6-8). These basidiomycete yeasts have
69 a global impact on human health because of their propensity to cause life-threatening
70 meningoencephalitis in immunocompromised hosts, including the HIV/AIDS
71 population, organ transplant recipients, and patients undergoing chemotherapy (9-11).
72 Key features of these species connected to mitochondrial activities and contributing to
73 disease include the formation of a polysaccharide capsule, titan cells, and the cell-wall
74 pigment melanin (12-14). These connections are demonstrated, for example, by the
75 reduction in capsule formation upon inhibition of the electron transport chain (ETC) in
76 *C. neoformans* and a fascinating "division of labour" role for mitochondria in *C. gattii*
77 (8, 15). In the latter case, a subset of fungal cells displays a tubular mitochondrial
78 morphology in response to oxidative stress provoked by the host. These cells support
79 the proliferation of other *C. gattii* cells with non-tubular organelle morphology within
80 host phagocytic cells. These results, combined with the role of mitochondria in
81 generating reactive oxygen species (ROS) (16-18), indicate a central role for the
82 organelle in fungal pathogenesis.

83 A number of additional studies demonstrate the role of mitochondria the
84 virulence of *C. neoformans*. For example, a mutation in the promoter of the gene
85 encoding mitochondrial complex I protein NADH dehydrogenase increases capsule and
86 melanin formation (19). Mutations in other regulatory factors also influence
87 mitochondrial functions and virulence. These include mutants lacking components of
88 the kinase module of the mediator complex (Cdk8 and Ssn801) that display altered
89 mitochondrial morphology, reduced growth on acetate, and impaired responses to
90 oxidative and cell wall stressors (6, 7). They also include mutants lacking the
91 transcription factors Mig1 or Gsb1 that demonstrate sensitivity to ETC inhibitors,
92 oxidative stress, and agents that challenge cell wall integrity (20, 21). In this context,

93 recent work identified the heat shock transcription factor Hsf3 as an important regulator
94 of ROS homeostasis in mitochondria, although mutants lacking the factor displayed
95 only minor attenuation of virulence in mice (22). This result is reminiscent of the
96 finding that HapX, another regulator of mitochondrial functions also plays a minor role
97 in virulence (23). Other factors that influence mitochondria in *C. neoformans* include
98 the temperature-responsive J domain protein Mrj1 that supports ETC function,
99 influences shedding of capsule polysaccharide, and impacts cell wall structure (24). A
100 detailed investigation revealed that Mrj1 plays a positive role in maintaining ETC
101 function at the complex III step.

102 Other mutants in *C. neoformans* display phenotypes that reinforce the known
103 connections between mitochondrial and iron homeostasis. These include mutants
104 lacking Vps45, a Sec1/Munc18 (SM) protein that participates in vesicle fusion; these
105 mutants have increased sensitivity to the ETC inhibitors SHAM (alternative oxidase),
106 antimycin A (complex III), and potassium cyanide (complex IV) (25). Additionally,
107 iron acquisition, cell wall integrity, mitochondrial function and virulence are dependent
108 on Vps45. Similarly, loss of the mitochondrial ABC transporter Atm1 which is required
109 for exporting an iron-sulfur (Fe-S) cluster precursor to the cytoplasm results in impaired
110 growth on non-fermentable carbon sources, enhanced sensitivity to oxidative stress,
111 reduced activity of the cytoplasmic Fe-S protein Leu1, and attenuated virulence in mice
112 (26). Atm1 also plays an important role in the response to copper toxicity that targets
113 Fe-S containing proteins (27).

114 During infection, pathogenic fungi use transcription factors to sense iron
115 availability and regulate iron transport and homeostasis, ensuring successful
116 competition for iron to support proliferation *in vivo* (28-30). We previously identified
117 Cir1 as an iron-responsive transcription factor in *C. neoformans* (28). Genetic studies
118 revealed that Cir1 is not only a master regulator of iron homeostasis but also regulates
119 key virulence factors including melanin and capsule. In particular, the *cir1Δ* mutant
120 exhibited markedly reduced infectivity, defective capsule production, and impaired
121 growth at 30°C or 37°C. By contrast, the mutant showed enhanced melanin production,
122 and this regulation is due in part to direct binding of Cir1 to the promoter of the laccase

123 gene *LAC1* and repression of transcription (28, 31). Melanin is deposited in the cell
124 wall and is a major virulence factor for *C. neoformans* that contributes to protection
125 against phagocytosis and oxidative killing by phagocytic cells (12, 13, 32-34). *C.*
126 *neoformans* synthesizes melanin from exogenous catecholamine substrates such as L-
127 3,4-dihydroxyphenylalanine (L-DOPA) through both laccase-catalyzed reactions and
128 spontaneous oxidation (33).

129 Cir1 is also a binding partner for the monothiol glutaredoxin Grx4 that
130 participates in iron homeostasis in *C. neoformans* (35). Additionally, mutation of the
131 glutaredoxin (GRX) domain of Grx4 results in defective melanin synthesis. Thus, Grx4
132 and Cir1 provide a key connection between iron homeostasis and melanin formation,
133 but the underlying signaling mechanisms are poorly understood. In other fungi, Grx4
134 also interacts with the HapX/Php4 component of the CCAAT binding complex (29,
135 36). This observation is consistent with the participation of HapX in iron homeostasis
136 in *C. neoformans* including repression of iron-dependent functions (e.g., mitochondrial
137 gene expression) upon iron limitation (23, 31). Loss of HapX also results in reduced
138 susceptibility to agents such as H_2O_2 and menadione that cause oxidative stress (20).
139 Our previous RNA-Seq and ChIP-Seq experiments revealed that *HAPX* is also a direct
140 target of Cir1 repression under iron replete conditions (23, 31). Thus, Cir1 and HapX
141 are key iron regulators that control iron homeostasis and mitochondrial functions in *C.*
142 *neoformans* (37). Furthermore, the pH responsive transcription factor Rim101 also
143 contributes to iron regulation in this pathogen (38, 39).

144 In this study, we examined the impact of ETC inhibition on melanin formation
145 and found a balancing influence of ROS and the activities of Cir1 and HapX. We also
146 established the influence of the melanin substrate L-DOPA, inhibition of ETC complex
147 III, or loss of Cir1 on the transcript levels of mitochondrial functions. Thus,
148 mitochondrial functions and the iron regulatory factors appear to both influence the
149 proper balance between oxidation and reduction to establish the conditions necessary
150 for melanin formation. In general, the regulation of melanization in fungi is complex
151 (13, 40-42), and our investigation adds new insights into connections between
152 mitochondrial function and virulence factor deployment.

153 **RESULTS**

154 **Inhibition of ETC complexes I and III impairs melanin formation.**

155 Given that melanin formation is influenced by a mutation in the gene for
156 mitochondrial NADH dehydrogenase, a component of complex I of the ETC (19), we
157 hypothesized that mitochondrial functions influence laccase expression, trafficking,
158 and/or activity. In particular, inhibition of ETC complexes I and III generates ROS
159 including superoxide anion radical and hydrogen peroxide, and the subsequent
160 influence on intracellular redox conditions may impact melanin formation (16-18, 22,
161 43). Additionally, mitochondria play important roles in metal ion homeostasis, heme
162 biosynthesis, and Fe-S cluster biogenesis that may influence the activity of regulatory
163 factors such as Cir1 which control laccase expression (31, 44). We investigated
164 mitochondrial contributions to melanin formation by examining pigment formation on
165 medium with L-DOPA and inhibitors of each ETC complex (Fig. 1A). We found that
166 melanin formation in the wild-type (WT) strain and the *cir1Δ* mutant was inhibited by
167 the complex I inhibitor rotenone, and that growth of the *cir1Δ* mutant was impaired on
168 rotenone compared with the other strains. A more striking reduction in melanin
169 accumulation was observed for the WT strain in the presence of the complex III
170 inhibitors antimycin A or myxothiazol (Fig. 1A). Interestingly, the impact of complex
171 III inhibitors on melanization was partially blocked in the *cir1Δ* and *hapXΔ* deletion
172 mutants (Fig. 1A). Additionally, the growth of the *cir1Δ* mutant was not markedly
173 impaired by antimycin A or myxothiazol compared to treatment with rotenone. A
174 mutant lacking the pH-responsive transcription factor Rim101 was included as a control
175 and did not influence melanin formation in the presence of ETC inhibitors. Overall, we
176 conclude that inhibition of ETC complex III activity impairs melanin formation, Cir1
177 and HapX influence the phenotypic impact of inhibition, and that inhibition of complex
178 I also has impact on melanin formation.

179

180 **Inhibition of ETC complex III impacts transcripts for mitochondrial functions,**
181 **but not laccase genes**

182 To investigate the connection between the ETC and melanin, we focused our
183 subsequent experiments on antimycin A and complex III inhibition by analyzing the
184 transcriptome of the WT strain treated with this inhibitor. In particular, we hypothesized
185 that an influence on the expression of *LAC1* (encoding the major laccase) or regulatory

186 factors for *LAC1* (e.g., Cir1) might account for the melanin defect. Our analysis
187 identified differential transcript levels for 210 genes, with 169 upregulated and 41
188 downregulated (Fig. S1). Moreover, subsequent analysis of gene ontology (GO) terms
189 revealed up regulation of molecular function categories associated with Fe-S cluster
190 and heme binding, and molecular carrier activity (Fig. 1B). These GO terms prompted
191 an analysis of transcript levels for components of the ETC as well as mitochondrial
192 (ISC) and cytoplasmic (CIA) Fe-S cluster assembly machinery to examine the impact
193 of ETC complex III inhibition. As shown in the heatmaps in Fig. 1C and Fig. S2A, we
194 found that inhibition resulted in elevated transcript levels for ETC components as well
195 as for functions for ISC and CIA machinery in the WT strain. Furthermore, the ETC
196 and mitochondrial ISC assembly pathways were found to be significantly enriched
197 through Gene Set Enrichment Analysis (GSEA). Table S1 lists the specific genes
198 represented by the heatmaps and Fig. S3 documents the output from the GSEA. The
199 RNA-Seq analysis revealed minimal impact of complex III inhibition on the transcript
200 levels of *LAC1* or *CIR1,* thus refuting our hypothesis.
201 We employed quantitative reverse transcription-PCR (qRT-PCR) to validate the
202 RNA-Seq data. This approach confirmed the transcript levels of the genes
203 CNAG_01881 and CNAG_05199 (ISC pathway genes), *ATM1* (mitochondrial ISC
204 transporter), and CNAG_05840 (CIA pathway gene) in agreement with the RNA-Seq
205 data (Fig. S2B). The transcript levels for the *LAC1* and *CIR1* genes were also confirmed
206 by qRT-PCR (Fig. S2B). A specific examination of the transcript levels for *LAC1,*
207 *CIR1, LAC2* (a second gene for laccase) and *HAPX* revealed that inhibition of ETC
208 complex III caused only modest reductions in mRNA levels for the *LAC1*, *LAC2,* and
209 *HAPX* genes, and a slight increase in mRNA levels for *CIR1* (Fig. S4). As mentioned,
210 our previous results showed that Cir1 directly and negatively regulates *LAC1* and *HAPX*
211 gene transcription (23, 31). Overall, we conclude that inhibition of complex III has a
212 major influence on transcript levels for mitochondrial functions involved in the ETC
213 and Fe-S biogenesis, but only a minor impact on transcript levels for the laccase genes
214 that is likely insufficient to explain the impaired melanin formation.
215
216 **Oxidative stress influences melanin formation**
217 Given the minor influence of antimycin A on *LAC1* and *LAC2* gene transcription
218 and the fact that the inhibitor triggers ROS in *C. neoformans* and other organisms (16-
219 18, 22, 43), we hypothesized that antimycin A influenced melanin by establishing redox

220 conditions that interfere with laccase activity. To support this idea, we examined the
221 transcript levels for genes responsive to oxidative stress and found that the transcript
222 levels for the *CAT1* and *CAT3* genes encoding catalases were elevated ~2 fold upon
223 antimycin A treatment (Table 1). The transcript levels for these genes are known to be
224 responsive to H_2O_2, among a larger group of oxidative stress genes (45). These
225 observations prompted a closer examination of the impact of ROS during melanin
226 formation and we found that the combination of H_2O_2 or menadione with the melanin
227 substrate L-DOPA impaired growth in liquid medium (Fig. 2A).
228 The connection with oxidative stress and redox homeostasis was examined further
229 by using a mutant known to influence the ETC at complex III and to have reduced ROS
230 levels. Specifically, we examined a mutant lacking the *MRJ1* gene encoding
231 mitochondrial respiration J-domain protein 1 that influences the activity of ETC
232 complex III by directly binding to Qcr2, a subunit of ubiquinol cytochrome c reductase
233 (24). We found that the effect of complex III inhibition on melanin formation was
234 partially blocked in the *mrj1*Δ mutant, a result consistent with the influence of Mrj1 on
235 ROS accumulation (Fig. 2B). These results further support the idea that melanin
236 formation is conditioned at least in part through a balance in redox homeostasis.
237
238 **L-DOPA negatively impacts the transcription of mitochondrial functions and**
239 **genes encoding catalases.**
240 Given that the combination of L-DOPA and H_2O_2 impaired growth, we
241 hypothesized that L-DOPA treatment might also influence oxidative stress and
242 mitochondrial functions. We therefore examined the impact of L-DOPA by performing
243 RNA-Seq to compare the transcript profiles for WT cells in the presence and absence
244 of L-DOPA. We found that L-DOPA treatment resulted in differential transcript levels
245 for 1,262 genes, with 836 upregulated and 426 downregulated (Fig. S5). Analysis of
246 the GO categories for the differentially transcribed genes indicated a negative impact
247 of L-DOPA treatment on functions associated with mitochondria (Fig. 3A). This
248 observation was further supported by GSEA using pathways from the KEGG database
249 and homologous gene IDs based on the genome of the *C. neoformans* strain JEC21.
250 This analysis revealed that 15 KEGG terms for mitochondrial functions, including ETC
251 components, were negatively enriched upon growth with L-DOPA (Fig. 3B). The
252 differential regulation of representative genes encoding ETC components (e.g., genes

253 CNAG_01287, CNAG_05041 and CNAG_07491) was confirmed by qRT-PCR (Fig.
254 S6). We also noted the transcript levels of genes encoding Cir1, HapX or Rim101 were
255 not differentially expressed in the RNA-Seq analysis of the response to L-DOPA, and
256 only a minor influence was observed by qRT-PCR (Fig. S6). A summary of the
257 differential transcript levels for mitochondrial functions is presented in Table S2. A
258 specific examination of the genes for oxidative stress (Table 1) also identified the
259 *CAT1, CAT2* and *CAT3* transcripts as being significantly elevated upon treatment with
260 L-DOPA. Together, these results revealed that conditions supporting melanin
261 formation (i.e., the presence of L-DOPA) have an impact on the expression of
262 mitochondrial functions as well as oxidative stress. These results reinforce the idea that
263 mitochondria are responsive to environmental signals, including L-DOPA, and control
264 ROS generation to establish conducive redox conditions that influence virulence factor
265 (melanin) production.
266
267 **Cir1 influences melanin formation through de-repression of *LAC1* transcription**
268 **and an influence of mitochondrial gene expression.**
269 As shown in Fig. 1A, complex III inhibitors impaired melanin formation in the WT
270 strain, and the *cir1Δ* and *hapXΔ* mutants partially restored melanin. Our previous
271 microarray, and RNA-Seq experiments with *cir1Δ* mutant demonstrated that Cir1
272 represses *LAC1* transcription (23, 31). Furthermore, ChiP-seq analysis revealed that
273 Cir1 directly binds the promoter of the *LAC1* gene to repress transcription (31). These
274 results suggest that de-repression upon loss of Cir1 during antimycin A treatment may
275 contribute to restored melanin formation. We therefore examined the influence of Cir1
276 on *LAC1* transcription, ETC function and oxidative stress genes by performing an
277 RNA-Seq experiment with WT and the *cir1Δ* mutant under the minimal medium
278 conditions used for the analysis of the impact of antimycin A on the transcriptome
279 (Materials & Methods). We identified 853 differentially expressed genes (710
280 upregulated and 143 downregulated) and an overview of the analysis is shown in Fig.
281 S7. As with previous transcriptome studies with Cir1 (23, 28, 31), an examination of
282 the GO terms for molecular functions that were upregulated in the *cir1Δ* mutant
283 revealed categories that included oxidoreductase activity (acting on peroxide as
284 acceptor, and acting on single donors with incorporation of molecular oxygen), Fe-S
285 cluster, copper ion binding, heme binding, antioxidant activity, transition metal iron

286 transmembrane transporter activity, and iron ion binding (Fig. 4). For example, the
287 transcript levels of mitochondrial ISC assembly machinery components were
288 significantly up-regulated in the *cir1Δ* mutant compared to the WT, and we note that
289 there are many Fe-S cluster binding proteins in complexes I, II and III of the ETC.
290 Additionally, genes encoding oxidative stress functions including the catalase genes
291 were up-regulated in the *cir1Δ* mutant (Table 1). Heatmaps of the regulation of
292 transcripts for ETC components and mitochondrial ISC assembly pathway components
293 in the *cir1Δ* mutant as compared to WT strain are shown in Fig. 4B and Fig.S8A; the
294 corresponding genes are listed in Table S3 and Fig. S9 presents the GSEA analysis of
295 the ETC and mitochondrial ISC pathways. Overall, these data confirm the influence of
296 Cir1 on mitochondrial functions - an affect that may impact susceptibility to complex
297 III inhibitors such as antimycin A through enhanced expression of specific organelle
298 transcripts.
299 To confirm the RNA-Seq data, the transcript levels of the ISC pathway gene
300 CNAG_03395, the ETC genes CNAG_06063, CNAG_07491 and CNAG_02839, and
301 *LAC1* were examined by qRT-PCR. We found comparable patterns of regulation
302 between the RNA-Seq and qRT-PCR results (Fig. S8B). Consistent with previous
303 analyses of the regulatory influence of Cir1 (23, 28, 31), we verified the differences
304 between the WT strain and the *cir1Δ* mutant for the transcript levels of the laccase genes
305 *LAC1* and *LAC2*, and confirmed the regulatory influence of Cir1 on the transcription of
306 the genes using qRT-PCR (Fig. S8C). Overall, these results suggest that loss of Cir1
307 leads to de-repression of *LAC1* to influence melanin in the presence of complex III
308 inhibitors. As mentioned above, an additional influence on the expression of
309 mitochondrial and oxidative stress functions may also condition susceptibility to ETC
310 inhibition.
311
312 **Cir1 and HapX respond differently to oxidative stress.**
313 In contrast to the regulation of *LAC1* expression by Cir1, previous experiments
314 revealed that HapX does not regulate laccase expression (23, 31). This observation
315 suggests a different mechanism for melanin recovery upon antimycin A treatment, and
316 we hypothesized that an influence of HapX on oxidative stress and the redox
317 environment impacts melanin formation. We therefore examined oxidative stress in
318 more detail by measuring ROS accumulation in the WT and *cir1Δ* and *hapXΔ* mutant

319 strains in response to antimycin A and myxothiazol treatment. Both mutants showed
320 higher levels of DCFDA staining compared to the WT strain indicating an accumulation
321 of ROS (Fig. 5A). The actions of multiple types of ROS (e.g., hydroxyl radicals, H_2O_2)
322 can oxidize DCFDA to generate a fluorescent signal (46). In contrast, staining with
323 dihydroethidium (DHE), which is responsive to superoxide accumulation revealed
324 greater levels in the *cir1Δ* mutant and lower endogenous levels/accumulation in the
325 *hapXΔ* mutant. The differences between the mutants prompted an examination of the
326 sensitivities of each strain to oxidative stress caused by H_2O_2, menadione, plumbagin
327 and paraquat (Fig. 6A). This experiment revealed greater sensitivity for the *cir1Δ*
328 mutant compared to the WT strain and the *hapXΔ* mutant. Consistent with this
329 differential sensitivity, we found that treatment with H_2O_2 provoked enhanced DCFDA
330 straining in the *cir1Δ* mutant but not in the WT strain or the *hapXΔ* mutant (Fig. 6B).
331 These observations are consistent with our previous finding that the *hapXΔ* mutant
332 behaves mainly like WT with regard to sensitivity to oxidative stress (20). HapX is
333 known to control the expression of functions for the response to oxidative stress,
334 including the *CAT1* and *CAT3* catalase genes influenced by antimycin A and L-DOPA
335 (Table 1) (23, 31). We confirmed this regulation by qRT-PCR for a set of the oxidative
336 stress genes from Table 1 (Fig. S10). Overall, these results suggest that antimycin A-
337 induced inhibition of melanin results from changes to the redox environment that are
338 unfavourable for melanin synthesis. Cir1 and particularly HapX appear to modulate this
339 influence by regulating the expression of antioxidant functions, along with the de-
340 repression of laccase expression upon loss of Cir1.
341
342 **DISCUSSION**
343 Melanin deposition in the cell wall of *C. neoformans* confers protection against
344 various stresses (e.g., oxidative killing by phagocytic cells) and reduces susceptibility
345 to antifungal drugs. These properties are relevant to disease because mutants with
346 defects in melanin formation show reduced virulence in mouse models, and melanin
347 influences dissemination to the brain and aspects of the immune response including
348 phagocytosis (13, 41). In this study, we examined the influence of impaired ETC
349 function on melanin formation with an emphasis on the response of WT cells to
350 antimycin A treatment, a condition known to increase ROS production (22). Given the
351 central role of mitochondria in iron homeostasis, we focused on the influence of iron

352 regulators on melanin formation upon mitochondrial impairment. We found that *cir1Δ*
353 and *hapXΔ* mutants lacking key iron regulators partially restored melanin in the
354 presence of ETC complex III inhibitors. These findings are consistent with our previous
355 discovery of negative regulation of laccase expression by Cir1, as well as the regulation
356 of genes for ETC components and oxidative stress functions by HapX (23, 31). Thus,
357 our analysis suggests two underlying mechanisms for the recovery of melanin in the
358 mutants upon antimycin A treatment: de-repression of *LAC1* by Cir1 and modulation
359 of the redox environment by Cir1 and HapX (Fig. 7). The proposed influence of HapX
360 is consistent with our previous finding of a reciprocal regulatory connection between
361 HapX and the candidate carbon catabolite repressor Mig1 in *C. neoformans* (20).
362 Notably, Mig1 regulates mitochondria functions, and the *mig1Δ* mutant was sensitive
363 to ETC inhibitors and inducers of ROS.

364 In addition to an influence on melanin, there are additional connections between
365 ETC activity and virulence factor expression in C. *neoformans*. For example, regulation
366 of polysaccharide capsule elaboration by ETC complexes I and III and alternative
367 oxidase (AOX) has been reported (15). Along with melanin, the polysaccharide capsule
368 is a major virulence factor for *C. neoformans* (47). Interestingly, ROS also influences
369 titan cell formation further highlighting the connections with virulence (14). These
370 observations reinforce the emerging view that mitochondrial activity is important for
371 fungi to resist host defenses and to cause disease, and are consistent with an impact of
372 iron levels on the size of the polysaccharide capsule and the expression of laccase (48-
373 50).

374 We focused on Cir1 in our analysis of the impact of ETC inhibition because of the
375 known repression of *LAC1* by the protein (23, 28, 31). Several studies have documented
376 melanin formation by *C. neoformans* in response to a variety of signals including
377 glucose levels, temperature, cell density, and metal ions (calcium, copper, iron) (49,
378 51). In this context, melanin formation is known to be regulated by a complex network
379 of transcription factors and kinases (42, 51). This network includes the transcription
380 factors Bzp4, Usv101, Mbs1, and Hob1 that activate *LAC1* transcription, and we
381 previously found that Cir1 directly regulates the transcription of *BZP4* (31). Thus, these
382 other factors may counter-balance the repression of *LAC1* by Cir1 to influence melanin
383 formation in response to different environmental and host conditions. Similarly, *HAPX*
384 transcription is also regulated by Cir1, and the influence of HapX on the oxidative stress

385 response was shown to affect melanin formation in the context of ETC inhibition. These
386 observations are consistent with HapX as a key regulator of oxidative stress functions
387 and iron-utilizing mitochondrial functions (23). Our analysis of the transcriptome in the
388 *cir1*Δ mutant also revealed regulation of mitochondrial functions and part of this
389 regulation may occur via an influence on HapX expression given that previous RNA-
390 Seq and ChIP-Seq did not identify the same pattern of regulation (31). The
391 transcriptional up-regulation of genes encoding mitochondrial components of the ETC
392 and iron-sulfur cluster synthesis observed for the *cir1*Δ mutant was similar to the
393 response to antimycin A treatment.

394 The observed regulation of oxidative stress functions by HapX and its known role
395 in regulating mitochondrial functions that use iron support the premise that
396 mitochondrial homeostasis orchestrates the necessary cellular environment for melanin
397 formation. The role of HapX in responding to and regulating redox conditions is
398 supported by orthologous studies in *Aspergillus* sp. and *S. cerevisiae* (52, 53). In
399 *Aspergillus nidulans*, for example, the CCAAT binding complex, of which HapX is a
400 regulatory subunit, is responsive to ROS via oxidation of key cysteine residues in a core
401 subunit. HapX in *C. neoformans* interacts with the core subunits of the CCAAT binding
402 complex (Hap2, 3 and 5) as demonstrated by DNA binding experiments (31). We note
403 that Cir1 and HapX also have cysteine-rich regions and ROS may potentially influence
404 the activities of these proteins via oxidation of cysteine residues. Additional
405 experiments are needed to investigate this possibility.

406 A key finding in our study was the connection between melanin, L-DOPA and
407 oxidative stress as demonstrated by the influence of H_2O_2 on growth in combination
408 with L-DOPA, and by the influence on melanin formation in an *mrj1*Δ mutant
409 previously demonstrated to have reduced ROS accumulation (24). Previously, the
410 transcriptional response of *C. neoformans* to H_2O_2 was analyzed and treatment resulted
411 in the decreased expression of the *LAC1* gene (45). Additionally, a set of genes was
412 identified that were responsive to H_2O_2 and that encode functions for oxidative stress
413 resistance. Together, these results support the idea that a balance of ROS is needed to
414 support melanin formation. However, the impact of ETC inhibition and ROS generation
415 is likely complex due to the multitude of potential targets of oxidative damage. For
416 example, we previously reported that Cir1 and HapX are both iron-binding proteins

417 (31), and iron or Fe-S cluster binding to these transcription factors might be affected by
418 inhibition of ETC complex III. Among the oxidative stress genes identified for *C.*
419 *neoformans* (45), the catalase genes appear to be regulated by antimycin A, L-DOPA
420 and HapX. However, the importance of catalase activity in this context is unclear
421 because a mutant lacking all four identified *CAT* genes is not defective for virulence in
422 mice (54). Oxidative stress in the context of fungal pathogenesis has recently been
423 reviewed (55).

424 Our analysis of cells exposed to L-DOPA revealed a substantial impact on the
425 transcriptome such that a large number of genes showed differential expression,
426 including the down-regulation of mitochondrial functions. This impact is interesting
427 because laccase activity and melanin may contribute to the neurotropism of *C.*
428 *neoformans* (56). The possibility that L-DOPA is a signal as well as a substrate is
429 intriguing because our observations of an influence on mitochondria draw parallels with
430 studies on the role of dopamine in neurons and in neurodegenerative diseases (57, 58).
431 For example, examination of the potential toxicity of L-DOPA in the treatment of
432 Parkinson's disease revealed an impact on mitochondrial and lysosomal activities (59).
433 A previous study examined the transcriptional response of *C. neoformans* to L-DOPA
434 using microarray analysis and, in contrast to our observations, found differential
435 expression of only eight genes (60). Some of these genes encoded functions predicted
436 to be involved in the response to stress and, importantly, this result is consistent with
437 our observed categories of GO terms and our demonstration that cells are more sensitive
438 to H_2O_2 in the presence of L-DOPA. The differences in the number of regulated genes
439 could be due to several factors including the use of microarray versus RNA-Seq
440 approaches (and associated differences in evaluating differential expression), the use of
441 different strains (JEC21 versus H99), different preculture conditions, and the timing
442 and level of L-DOPA exposure. However, four of the JEC21 genes had regulated
443 orthologs in the RNA-Seq data for H99. Interestingly, regulation of five of the genes
444 was not observed in a laccase mutant suggesting that formation of melanin may have a
445 regulatory influence (60, 61).

446 In summary, we have established that impaired ETC complex III activity influences
447 the elaboration of melanin in *C. neoformans* and that iron regulatory factors buffer this
448 influence. Other proteins in the iron regulatory network influence melanin formation in
449 addition to Cir1 and HapX. For example, the monothiol glutaredoxin Grx4 interacts
450 with Cir1 and HapX and has a positive influence on melanin formation (along many
451 other phenotypic contributions such as cell wall integrity) (62). Thus, additional work
452 is needed to investigate the influence of Grx4 on melanin, potentially in partnership
453 with Cir1, HapX and other regulatory proteins. Finally, we also found that L-DOPA
454 treatment impacts the expression of mitochondrial functions thus warranting an
455 investigation into a potential signaling role for this important substrate.

456 **MATERIALS AND METHODS**

457 **Strains, growth conditions, and spot assays with inhibitors.** The following strains
458 were used in this study: WT strain *Cryptococcus neoformans* var. *grubii* H99, deletion
459 mutants *cir1*Δ (28), *hapX*Δ (23), *rim101*Δ (63, 64), *atm1*Δ (26), and *mrj1*Δ (16) (24),
460 and complemented mutants *cir1*Δ::*CIR1* (28), *hapX*Δ::*HAPX* (23), *rim101*Δ::*RIM101*
461 (63, 64), *atm1*Δ::*ATM1-GFP* (26), and *mrj1*Δ::*MRJ1-GFP* (24). Routine growth was in
462 YPD or YNB liquid or solid media.

463 Melanin production was examined in medium with L-DOPA (0.1% glucose, 0.1%
464 L-asparagine, 0.3% KH_2PO_4, 0.7 mM L-DOPA, 0.025%MgSO4 · $7H_2O$, pH 5.6). Agar
465 was added at 2% for solid medium. For spot assays, cells from overnight cultures at
466 30°C were washed twice with liquid YPD medium, density was adjusted to 1×10^5 cells
467 ml^{-1} and 10-fold serial dilutions were prepared. Next, 5 µl was spotted on the 2% L-
468 DOPA agar plates with or without the ETC inhibitors at the indicated concentrations.
469 Plates were incubated in the dark for 72 h at 30°C, and photographed to document
470 melanin formation.

471 To examine *C. neoformans* WT (H99) or mutant strains, cells were grown in YPD
472 or YNB for ~16 hours at 30°C. Precultures were washed, resuspended in H_2O and 10-
473 fold serial dilutions were performed from an initial concentration of 2 x 10^7 cells per
474 milliliter. Five µl were spotted into solid YPD or YNB plates supplemented with
475 different compounds and incubated at 30°C and 37°C for 2-3 days before being
476 scanned. For the reactive oxygen stress response, rich (YPD) and minimal (YNB)
477 media were supplemented with the following compounds: hydrogen peroxide solution
478 (H_2O_2, 1-5 mM), menadione (10, 15 µg/ml), plumbagin (50, 100 µM), paraquat (0.25,
479 0.35 mM).
480

481 **RNA extraction, RNA sequencing and analysis, and quantitative reverse**
482 **transcription-PCR.** To examine the impact of complex III inhibition on the
483 transcriptome, the WT strain and the *cir1*Δ and *hapX* Δ mutants were grown in 50 ml
484 of YPD at 30°C for 16 h. The cells were washed twice with sterile water and then
485 incubated in 50 ml of YNB with 0.06% glucose for 16 h at 30°C. The cells were then
486 diluted to 4.0 x 10^7 cells in 50 ml of YNB medium (2% glucose) with or without 0.5
487 µg/ml antimycin A, followed by a 6 h incubation at 30°C. For the analysis of the
488 influence of L-DOPA on the transcriptome, three replicate cultures of WT cells were
489 grown in 50 ml of YPD (2% glucose) at 30°C for 16 h. Cells were then washed twice
490 with sterile water, and diluted to 4.0 x 10^7 cells in 50 ml of melanin induction medium
491 with or without 0.7 mM L-DOPA. After incubation for 6 h at 30°C, the cells were
492 harvested and flash frozen in liquid nitrogen. The total RNA from frozen cells was
493 extracted by using RNeasy-Mini kit (QIAGEN), followed by treatment with DNase I
494 (TURBO DNA-free™ Kit). RNA-Seq was performed by Genewiz (Azenta Life
495 Sciences, South Plainfield, NJ, USA).

496 Differentially expressed genes were analyzed in R (version 4.3.2) using the raw
497 gene counts provided from Genewiz and the DEseq2 package. All genes were assessed

498 for significance using DEseq2's inherent Wald test (pvalue cut-off = 0.05) and
499 normalized between samples using the median of ratios method (65). The identification
500 of enriched pathways was performed by two independent approaches. First, to identify
501 significantly enriched functional groups, the RNA-Seq data were analyzed with respect
502 to KEGG database annotations. For compatibility with the KEGG database, FungiDB
503 was used to convert gene ID's from strain H99 to strain JEC21. Based on both a ranked
504 genelist (Ranked score = -(log2FoldChange) x log10 (p value)) derived from the
505 DESeq2 output and the KEGG/PATHWAY database, the identification of enriched
506 pathways was performed by Gene Set Enrichment Analysis (GSEA) with 10,000
507 permutations (66). The output was visualized using Enrichment Map with a Benjamini
508 Hochberg FDR value of 0.25, and a *P*-value cut-off of 0.05 for all comparisons. Gene
509 sets between 10 and 400 were included (67). Gene sets were visualized in heatmaps of
510 the normalized expression generated using R (68) and the DittoSeq package (Bunis et
511 al., 2021). Clustering was performed to organize samples and genes of similar
512 expression (69). Second, we also analyzed sets of over-represented pathways for
513 enrichment in protein functions. *De novo* Gene Ontology (GO) term assignments of
514 predicted proteins were performed by InterProScan 5.26-65 (70). We kept the GO terms
515 with a total term size in the genome of at least five. To test for enrichment, we
516 performed hypergeometric tests. GO terms were only considered significant if the FDR
517 *P*-values were less than <0.001. The R packages GSEABase (71) and GOstats (72) were
518 used to analyze all enrichments, and the R package ggplot2 (73) was used to visualize
519 the outcomes of enrichment tests. Gene expression in the samples for RNA-Seq was
520 verified by qRT-PCR following published procedures (74). The primers for qPCR
521 validation are listed in Table S4.

522 **RNA extraction and qPCR to analyze oxidative stress**

523 Overnight grown wild type (H99) and *hapXΔ* cells (2.5 mL) in YPD media were washed
524 thrice with low iron water and incubated in 50 mL of YNB media supplemented with
525 BPS (150 μM) for 24 hours at 30°C and 140-150 rpm. Subsequently, cultures were
526 collected, washed twice with YNB-BPS and 500 μL of cells resuspensions were treated
527 in YNB-BPS for 1 hours at 30 C ~220 rpm. Cells were harvested, washed with ice cold
528 low iron water and pellets were frozen in liquid nitrogen and kept at -80°C. Total RNA
529 was extracted from lysed cells using the RNeasy ® Mini kit (Qiagen) and DNA was
530 removed using Turbo DNA-*free*™ Kit (Invitrogen). Synthesis of cDNA was obtained
531 using the High-Capacity cDNA Reverse Transcription Kit (Applied Biosystems ™)
532 using oligo (dT). Real-time PCR (qPCR) was performed using the primers listed in
533 Supplementary Table S5, cDNA and Green-2-Go qPCR Mastermix-low Rox
534 (BioBasic) as described by the manufacturer. Samples were run on an Applied
535 Biosystems 7500 Fast real-time PCR System. Relative gene expression was quantified
536 using the ΔCT method normalized to *ACT1* gene. Statistical analysis was performed
537 using two-way ANOVA test followed by a *post hoc* Šídák's multiple comparison test.
538

539 **Flow cytometry analysis**

540 Flow cytometric measurements were performed using CytoFLEX S (Beckman Coulter)
541 Flow Cytometer equipped with four laser lines (405 nm, 488 nm, 561 nm and 633 nm)
542 fitted with filters FITC (525/40) and PE (585/42). The number of cells measured per
543 experiment was set to 30,000-40,000 unless otherwise stated. For the study of
544 mitochondrial related ROS under the influence of ETC III inhibition, cells were grown
545 overnight at ~200 rpm and 30°C in YPD media and washed twice with PBS.
546 Subsequently, 0.3 OD cells were grown on minimal media (YNB) for 24 hours and then
547 treated in YNB media with and without the ETC III inhibitors antimycin A (AA, 50
548 μM) or myxothiazol (Myx, 7 μM) for 24 h at 200 rpm and 30°C. After treatment cells
549 were stained with the intracellular reactive oxygen species (ROS) detector 2′,7′-
550 Dichlorofluorescein Diacetate (DCFDA, 16 μM; Sigma-Aldrich) or Dihydroethidium
551 (DHE, 2.5 μg/ml; EMD Millipore Corp.) for 1 h at 30°C. For the analysis upon ROS

552 stressors, cells were grown on YPD media overnight as mentioned above. Next, cells
553 were grown in YNB media and collected on log phase to subsequently treat them with
554 or without hydrogen peroxide solution (H_2O_2, 5 mM; Sigma-Aldrich) for 1 hour at
555 30°C. Afterwards, cells were washed with PBS and stained with DCFDA as mentioned
556 above. Data analysis and evaluation was conducted using FlowJo software version
557 (10.8.2; 2006-2022). The gating strategy for cryptococcus cells is depicted in Fig. S11.
558 Statistical analysis involved conducting a two-way ANOVA test, followed by *post hoc*
559 Šídák's or Tukey's multiple comparison tests. GraphPad Prism software was utilized
560 for the statistical analysis.
561

562 **Data availability.** The RNA-Seq data have been deposited in Gene Expression
563 Omnibus record GSE222564. The full gene lists for the RNA-Seq data for each
564 condition are given in Supplemental Tables S6-S8

565 **ACKNOWLEDGMENTS**

566 Research reported in this publication was supported by the National Institute of Allergy
567 and Infectious Diseases of the National Institutes of Health under Award Number
568 R01AI053721 (to J.W.K.). The content is solely the responsibility of the authors and
569 does not necessarily represent the official views of the National Institutes of Health.
570 J.W.K. is a Burroughs Wellcome Fund Scholar in Molecular Pathogenic Mycology and
571 the Power Corporation fellow of the CIFAR program: Fungal Kingdom, Threats &
572 Opportunities.

573 P.X., E.S.-L., W.J., and J.W.K. designed the study and P.X., E.S.-L., G.H. and B.B.
574 performed the microbiological and transcriptome experiments. H.L. performed qRT-
575 PCR experiments. P.X., E.S.-L., C.W.J.L. B.B., A.B. and J.W.K. performed data
576 analysis. P.X., E.S.-L., W.J. and J.W.K. wrote the manuscript with input from all
577 authors.

578 **CONFLICT OF INTEREST**

579 The authors declare no competing interests.

580

581 REFERENCES
582

583 1. Ma H, Hagen F, Stekel DJ, Johnston SA, Sionov E, Falk R, Polacheck I, Boekhout
584 T, May RC. 2009. The fatal fungal outbreak on Vancouver Island is characterized by
585 enhanced intracellular parasitism driven by mitochondrial regulation. Proc Natl Acad
586 Sci USA 106:12980-12985.
587

588 2. Calderone R, Li D, Traven A. 2015. System-level impact of mitochondria on fungal
589 virulence: to metabolism and beyond. FEMS Yeast Res. 15(4):fov027.
590

591 3. Verma S, Shakya VPS, Idnurm A. 2018. Exploring and exploiting the connection
592 between mitochondria and the virulence of human pathogenic fungi. Virulence.
593 9:426-446.
594

595 4. Black B, Lee C, Horianopoulos LC, Jung WH, Kronstad JW. 2021. Respiring to
596 infect: Emerging links between mitochondria, the electron transport chain, and fungal
597 pathogenesis. PLoS Pathog. 17:e1009661.
598

599 5. Kretschmer M, Damoo D, Sun S, Lee CW, Croll D, Brumer H, Kronstad J. 2022.
600 Organic acids and glucose prime late-stage fungal biotrophy in maize. Science
601 376:1187-1191.
602

603 6. Chang AL, Doering TL. 2018. Maintenance of mitochondrial morphology in
604 *Cryptococcus neoformans* is critical for stress resistance and virulence. MBio
605 9:e01375-18.
606

607 7. Chang AL, Kang Y, Doering TL. 2019. Cdk8 and Ssn801 regulate oxidative stress
608 resistance and virulence in *Cryptococcus neoformans*. MBio 10:e02818-18.
609

610 8. Voelz K, Johnston SA, Smith LM, Hall RA, Idnurm A, May RC. 2014. 'Division
611 of labour'in response to host oxidative burst drives a fatal *Cryptococcus gattii*
612 outbreak. Nat Commun 5:1-12.
613
614 9. Rajasingham R, Smith RM, Park BJ, Jarvis JN, Govender NP, Chiller TM,
615 Denning DW, Loyse A, Boulware DR. 2017. Global burden of disease of HIV-
616 associated cryptococcal meningitis: an updated analysis. Lancet Infect Dis 17:873-
617 881.
618
619 10. Okurut S, Boulware DR, Olobo J, Meya DB. 2020. Landmark clinical
620 observations and immunopathogenesis pathways linked to HIV and Cryptococcus
621 fatal central nervous system co-infection. Mycoses 63:840-853.
622
623 11. Tugume L, Ssebambulidde K, Kasibante J, Ellis J, Wake RM, Gakuru J, Lawrence
624 DS, Abassi M, Rajasingham R, Meya DB, Boulware DR. 2023. Cryptococcal
625 meningitis. Nat Rev Dis Primers. 9:62.
626
627 12. Zaragoza O. 2019. Basic principles of the virulence of Cryptococcus. Virulence
628 10:490-501.
629
630 13. Liu S, Youngchim S, Zamith-Miranda D, Nosanchuk JD. 2021. Fungal melanin
631 and the mammalian immune system. J Fungi 7:264.
632
633 14. García-Barbazán I, Torres-Cano A, García-Rodas R, Sachse M, Luque D, Megías
634 D, Zaragoza O. 2024. Accumulation of endogenous free radicals is required to induce
635 titan-like cell formation in *Cryptococcus neoformans*. mBio. 15:e0254923.
636
637 15. Trevijano-Contador N, Rossi SA, Alves E, Landín-Ferreiroa S, Zaragoza O. 2017.
638 Capsule enlargement in *Cryptococcus neoformans* is dependent on mitochondrial
639 activity. Front Microbiol 8:1423.
640

641 16. Pham NA, Robinson BH, Hedley DW. 2000. Simultaneous detection of
642 mitochondrial respiratory chain activity and reactive oxygen in digitonin-
643 permeabilized cells using flow cytometry. Cytometry A: 41:245-251.
644
645 17. Lenaz G. 2001. The mitochondrial production of reactive oxygen species:
646 mechanisms and implications in human pathology. IUBMB Life. 52:159-164.
647
648 18. Brand MD, Nicholls DG. 2011. Assessing mitochondrial dysfunction in cells.
649 Biochem J. 435:297-312.
650
651 19. Merryman M, Crigler J, Seipelt-Thiemann R, McClelland E. 2020. A mutation in
652 *C. neoformans* mitochondrial NADH dehydrogenase results in increased virulence in
653 mice. Virulence 11:1366-1378.
654
655 20. Caza M, Hu G, Price M, Perfect JR, Kronstad JW. 2016. The zinc finger protein
656 Mig1 regulates mitochondrial function and azole drug susceptibility in the pathogenic
657 fungus *Cryptococcus neoformans*. mSphere. 1:e00080-15.
658
659 21. Cheon SA, Thak EJ, Bahn Y-S, Kang HA. 2017. A novel bZIP protein, Gsb1, is
660 required for oxidative stress response, mating, and virulence in the human pathogen
661 *Cryptococcus neoformans*. Sci Rep 7:1-15.
662
663 22. Gao X, Fu Y, Sun S, Gu T, Li Y, Sun T, Li H, Du W, Suo C, Li C. 2022.
664 Cryptococcal Hsf3 controls intramitochondrial ROS homeostasis by regulating the
665 respiratory process. Nat Commun 13:1-16.
666
667 23. Jung WH, Saikia S, Hu GG, Wang J, Fung CK-Y, D'Souza C, White R, Kronstad
668 JW. 2010. HapX positively and negatively regulates the transcriptional response to
669 iron deprivation in *Cryptococcus neoformans*. PloS Pathog 6:e1001209.
670
671 24. Horianopoulos LC, Hu G, Caza M, Schmitt K, Overby P, Johnson JD, Valerius O,
672 Braus GH, Kronstad JW. 2020. The novel J-domain protein Mrj1 is required for

673 mitochondrial respiration and virulence in *Cryptococcus neoformans*. MBio
674 11:e01127-20.
675
676 25. Caza M, Hu G, Nielson ED, Cho M, Jung WH, Kronstad JW. 2018. The
677 Sec1/Munc18 (SM) protein Vps45 is involved in iron uptake, mitochondrial function
678 and virulence in the pathogenic fungus *Cryptococcus neoformans*. PLoS Pathog
679 14:e1007220.
680
681 26. Do E, Park S, Li MH, Wang JM, Ding C, Kronstad JW, Jung WH. 2018. The
682 mitochondrial ABC transporter Atm1 plays a role in iron metabolism and virulence in
683 the human fungal pathogen *Cryptococcus neoformans*. Med Mycol 56:458-468.
684
685 27. Garcia-Santamarina S, Uzarska MA, Festa RA, Lill R, Thiele DJ. 2017.
686 *Cryptococcus neoformans* iron-sulfur protein biogenesis machinery is a novel layer of
687 protection against Cu stress. mBio 8:e01742-17.
688
689 28. Jung WH, Sham A, White R, Kronstad JW. 2006. Iron regulation of the major
690 virulence factors in the AIDS-associated pathogen *Cryptococcus neoformans*. PLoS
691 Biol 4:e410.
692
693 29. Gupta M, Outten CE. 2020. Iron–sulfur cluster signaling: The common thread in
694 fungal iron regulation. Curr Opin Chem Biol 55:189-201.
695
696 30. Misslinger M, Hortschansky P, Brakhage AA, Haas H. 2021. Fungal iron
697 homeostasis with a focus on *Aspergillus fumigatus*. Biochim Biophys Acta Mol Cell
698 Res 1868:118885.
699
700 31. Do E, Cho YJ, Kim D, Kronstad JW, Jung WH. 2020. A transcriptional regulatory
701 map of iron homeostasis reveals a new control circuit for capsule formation in
702 *Cryptococcus neoformans*. Genetics 215:1171-1189.
703
704 32. Wang Y, Aisen P, Casadevall A. 1995. *Cryptococcus neoformans* melanin and
705 virulence: mechanism of action. Infect Immun 63:3131-3136.
706

707 33. Kwon-Chung K, Tom W, Costa J. 1983. Utilization of indole compounds by
708 *Cryptococcus neoformans* to produce a melanin-like pigment. J Clin Microbiol
709 18:1419-1421.
710
711 34. Panepinto JC, Williamson PR. 2006. Intersection of fungal fitness and virulence in
712 *Cryptococcus neoformans*. FEMS Yeast Res 6:489-498.
713
714 35. Attarian R, Hu GG, Sánchez-León E, Caza M, Croll D, Do E, Bach H, Missall T,
715 Lodge J, Jung WH. 2018. The monothiol glutaredoxin Grx4 regulates iron
716 homeostasis and virulence in *Cryptococcus neoformans*. MBio 9:e02377-18.
717
718 36. Dlouhy AC, Beaudoin J, Labbé S, Outten CE. 2017. *Schizosaccharomyces pombe*
719 Grx4 regulates the transcriptional repressor Php4 via [2Fe–2S] cluster binding.
720 Metallomics 9:1096-1105.
721
722 37. Jung WH, Sánchez-León E, Kronstad JW. 2021. Coordinated regulation of iron
723 metabolism in *Cryptococcus neoformans* by GATA and CCAAT transcription factors:
724 connections with virulence. Curr Genet 67:583-593.
725
726 38. O'Meara TR, Norton D, Price MS, Hay C, Clements MF, Nichols CB, Alspaugh
727 JA. 2010. Interaction of *Cryptococcus neoformans* Rim101 and protein kinase A
728 regulates capsule. PLoS Pathog 6:e1000776.
729
730 39. O'Meara TR, Xu W, Selvig KM, O'Meara MJ, Mitchell AP, Alspaugh JA. 2014.
731 The *Cryptococcus neoformans* Rim101 transcription factor directly regulates genes
732 required for adaptation to the host. Mol Cell Biol 34:673-684.
733
734 40. Idnurm A. 2011. New surprises from within the black box of fungal melanization.
735 Virulence. 2:261-263.
736
737 41. Smith DFQ, Casadevall A. 2019. The role of melanin in fungal pathogenesis for
738 animal hosts. Curr Top Microbiol Immunol. 422:1-30.
739

740 42. Lee D, Jang E-H, Lee M, Kim S-W, Lee Y, Lee K-T, Bahn Y-S. 2019. Unraveling
741 melanin biosynthesis and signaling networks in *Cryptococcus neoformans*. mBio
742 10:e02267-19.
743
744 43. Bolter CJ, Chefurka W. 1990. Extramitochondrial release of hydrogen peroxide
745 from insect and mouse liver mitochondria using the respiratory inhibitors phosphine,
746 myxothiazol, and antimycin and spectral analysis of inhibited cytochromes. Arch
747 Biochem Biophys. 278:65-72.
748
749 44. Monzel AS, Enríquez JA, Picard M. 2023. Multifaceted mitochondria: moving
750 mitochondrial science beyond function and dysfunction. Nat Metab. 5:546-562.
751
752 45. Upadhya R, Campbell LT, Donlin MJ, Aurora R, Lodge JK. 2013. Global
753 transcriptome profile of *Cryptococcus neoformans* during exposure to hydrogen
754 peroxide induced oxidative stress. PloS One 8:e55110.
755
756 46. Shehat MG, Tigno-Aranjuez J. 2019. Flow cytometric measurement of ROS
757 production in Macrophages in response to FcγR cross-linking. J Vis Exp.
758 7:10.3791/59167.
759
760 47. Casadevall A, Coelho C, Cordero RJB, Dragotakes Q, Jung E, Vij R, Wear MP.
761 2019. The capsule of *Cryptococcus neoformans*. Virulence. 10:822-831.
762
763 48. Jacobson E, Compton G. 1996. Discordant regulation of phenoloxidase and
764 capsular polysaccharide in *Cryptococcus neoformans*. J Med Vet Mycol 34:289-291.
765
766 49. Zhu X, Williamson PR. 2004. Role of laccase in the biology and virulence of
767 Cryptococcus neoformans. FEMS Yeast Res 5:1-10.
768
769 50. Vartivarian SE, Anaissie EJ, Cowart RE, Sprigg HA, Tingler MJ, Jacobson ES.
770 1993. Regulation of cryptococcal capsular polysaccharide by iron. J Infect Dis
771 167:186-190.

51. Cordero RJ, Camacho E, Casadevall A. 2020. Melanization in *Cryptococcus neoformans* requires complex regulation. mBio 11:e03313-19.

52. Hortschansky P, Haas H, Huber EM, Groll M, Brakhage AA. 2017. The CCAAT-binding complex (CBC) in *Aspergillus* species. Biochim Biophys Acta Gene Regul Mech. 1860:560-570.

53. Chevtzoff C, Yoboue ED, Galinier A, Casteilla L, Daignan-Fornier B, Rigoulet M, Devin A. 2010. Reactive oxygen species-mediated regulation of mitochondrial biogenesis in the yeast *Saccharomyces cerevisiae*. J Biol Chem. 285:1733-1742.

54. Giles SS, Stajich JE, Nichols C, Gerrald QD, Alspaugh JA, Dietrich F, Perfect JR. 2006. The *Cryptococcus neoformans* catalase gene family and its role in antioxidant defense. Eukaryot Cell. 5:1447-1459.

55. Warris A, Ballou ER. 2019. Oxidative responses and fungal infection biology. Semin Cell Dev Biol. 89:34-46.

56. Berg SZ, Berg J. 2023. Melanin: a unifying theory of disease as exemplified by Parkinson's, Alzheimer's, and Lewy body dementia. Front Immunol. 14:1228530.

57. Billings JL, Gordon SL, Rawling T, Doble PA, Bush AI, Adlard PA, Finkelstein DI, Hare DJ. 2019. l-3, 4-dihydroxyphenylalanine (l-DOPA) modulates brain iron, dopaminergic neurodegeneration and motor dysfunction in iron overload and mutant alpha-synuclein mouse models of Parkinson's disease. J Neurochem 150:88-106.

58. Burbulla LF, Song P, Mazzulli JR, Zampese E, Wong YC, Jeon S, Santos DP, Blanz J, Obermaier CD, Strojny C. 2017. Dopamine oxidation mediates mitochondrial and lysosomal dysfunction in Parkinson’s disease. Science 357:1255-1261.

803 59. Graves SM, Xie Z, Stout KA, Zampese E, Burbulla LF, Shih JC, Kondapalli J,
804 Patriarchi T, Tian L, Brichta L. 2020. Dopamine metabolism by a monoamine oxidase
805 mitochondrial shuttle activates the electron transport chain. Nature Neurosci 23:15-
806 20.
807
808 60. Eisenman HC, Chow S-K, Tsé KK, McClelland E, Casadevall A. 2011. The effect
809 of L-DOPA on *Cryptococcus neoformans* growth and gene expression. Virulence
810 2:329-336.
811
812 61. Idnurm A. 2011. New surprises from within the black box of fungal melanization.
813 Virulence. 2:261-263.
814
815 62. Hu G, Horianopoulos L, Sánchez-León E, Caza M, Jung W, Kronstad JW. 2021.
816 The monothiol glutaredoxin Grx4 influences thermotolerance, cell wall integrity, and
817 Mpk1 signaling in *Cryptococcus neoformans*. G3 (Bethesda) 11:jkab322.
818
819 63. Hu G, Caza M, Cadieux B, Chan V, Liu V, Kronstad J. 2013. *Cryptococcus*
820 *neoformans* requires the ESCRT protein Vps23 for iron acquisition from heme, for
821 capsule formation, and for virulence. Infect Immun. 81:292-302.
822
823 64. Hu G, Caza M, Cadieux B, Bakkeren E, Do E, Jung WH, Kronstad JW. 2015. The
824 endosomal sorting complex required for transport machinery influences haem uptake
825 and capsule elaboration in *Cryptococcus neoformans*. Mol Microbiol 96:973-992.
826
827 65. Love MI, Huber W, Anders S. 2014. Moderated estimation of fold change and
828 dispersion for RNA-seq data with DESeq2. Genome Biol 15:1-21.
829
830 66. Subramanian A, Tamayo P, Mootha VK, Mukherjee S, Ebert BL, Gillette MA,
831 Paulovich A, Pomeroy SL, Golub TR, Lander ES. 2005. Gene set enrichment
832 analysis: a knowledge-based approach for interpreting genome-wide expression
833 profiles. Proc Natl Acad Sci USA 102:15545-15550.
834

835 67. Merico D, Isserlin R, Stueker O, Emili A, Bader GD. 2010. Enrichment map: a
836 network-based method for gene-set enrichment visualization and interpretation. PloS
837 One 5:e13984.
838
839 68. Team RC. 2022. R: A Language and Environment for Statistical Computing. R
840 Foundation for Statistical Computing, Vienna, Austria. https://www.R-project.org/.
841
842 69. Bunis DG, Andrews J, Fragiadakis GK, Burt TD, Sirota M. 2021. dittoSeq:
843 universal user-friendly single-cell and bulk RNA sequencing visualization toolkit.
844 Bioinform 36:5535-5536.
845
846 70. Jones P, Binns D, Chang H-Y, Fraser M, Li W, McAnulla C, McWilliam H,
847 Maslen J, Mitchell A, Nuka G. 2014. InterProScan 5: genome-scale protein function
848 classification. Bioinform 30:1236-1240.
849
850 71. Martin M, Seth F, Robert G. 2021. GSEABase: Gene set enrichment data
851 structures and methods. R package version 1.56.0.
852
853 72. Falcon S, Gentleman R. 2007. Using GOstats to test gene lists for GO term
854 association. Bioinform 23:257-258.
855
856 73. Wickham H. 2009. ggplot2; Elegant graphics for data analysis. P 1-213. *In*
857 Applied Spatial Data Analysis R. Springer New York, NY.
858
859 74. Horianopoulos LC, Lee CW, Schmitt K, Valerius O, Hu G, Caza M, Braus GH,
860 Kronstad JW. 2021. A J domain protein functions as a histone chaperone to maintain
861 genome integrity and the response to DNA damage in a human fungal pathogen. mbio
862 12:e03273-21.

Figure 1

A

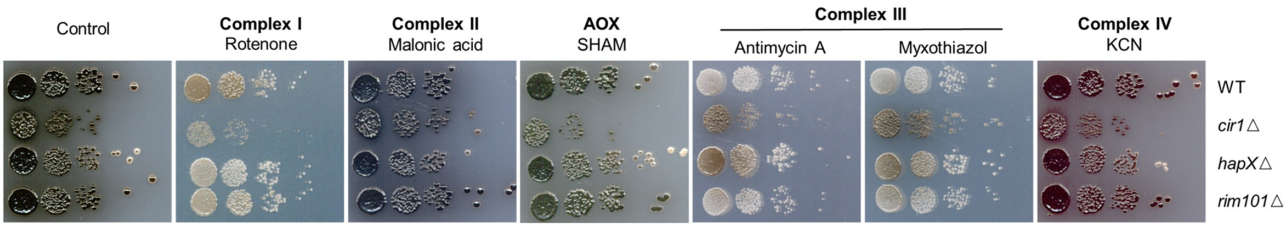
Control
Complex I
Rotenone
Complex II
Malonic acid
AOX
SHAM
Complex III
Antimycin A
Myxothiazol
Complex IV
KCN
WT
cir1△
hapX△
rim101△

B

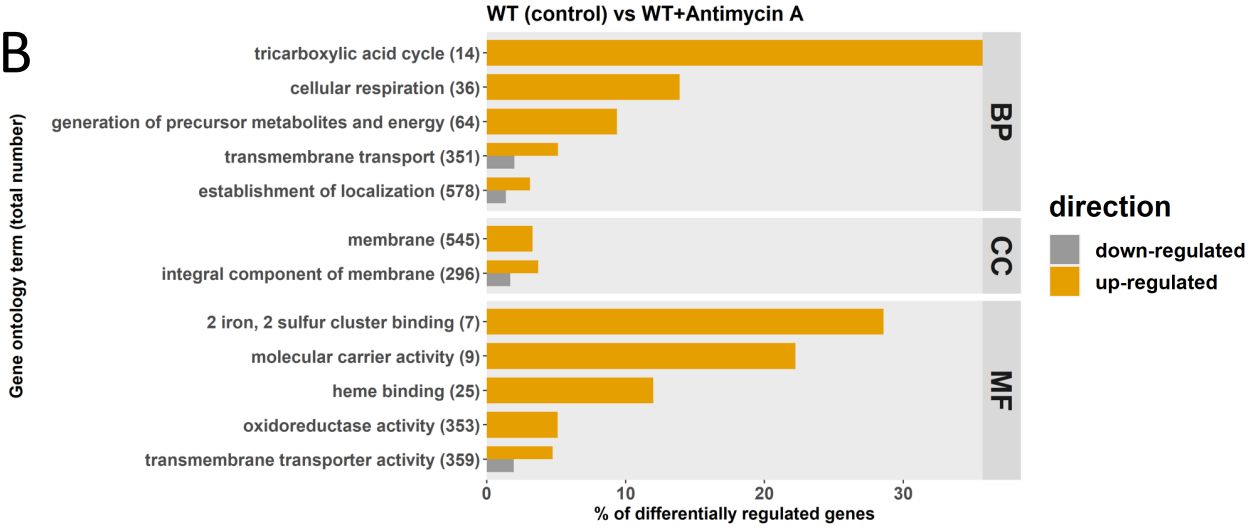
WT (control) vs WT+Antimycin A
Gene ontology term (total number)
tricarboxylic acid cycle (14)
cellular respiration (36)
generation of precursor metabolites and energy (64)
transmembrane transport (351)
establishment of localization (578)
membrane (545)
integral component of membrane (296)
2 iron, 2 sulfur cluster binding (7)
molecular carrier activity (9)
heme binding (25)
oxidoreductase activity (353)
transmembrane transporter activity (359)
BP
CC
MF
0
10
20
30
% of differentially regulated genes
direction
down-regulated
up-regulated

C

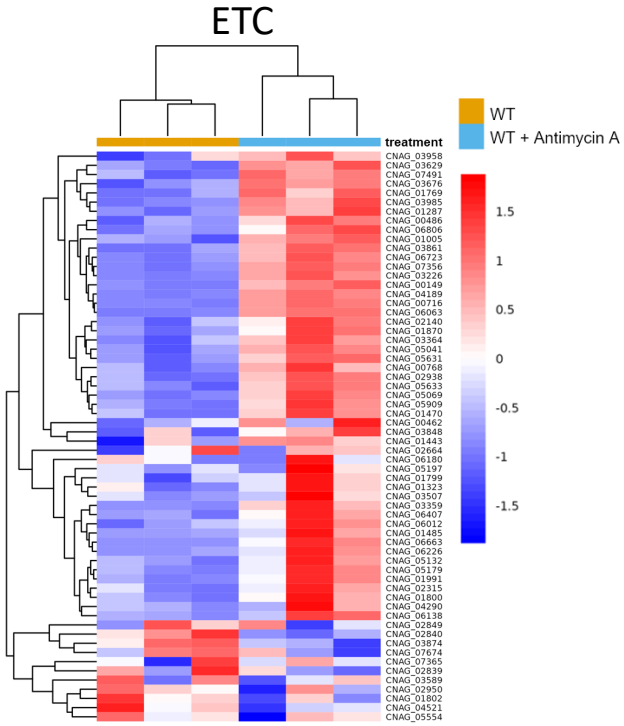
ETC
treatment
WT
WT + Antimycin A
1.5
1
0.5
0
-0.5
-1
-1.5

FIG 1 ETC inhibition influences melanin formation and the transcription of genes for mitochondrial functions. (**A**) Spot assays of WT and mutant strains on L-DOPA agar plates with or without inhibitors of the ETC including 1.2 μg/ml rotenone, 100 μM malonic acid, 0.2 mM salicylhydroxamic acid (SHAM), 0.5 μg/ml antimycin A, 0.5 μM myxothiazol, and 100 μM KCN. Plates were incubated for 72 h at 30° C in the dark. (**B**) Gene ontology (GO) categories of the differentially expressed genes identified by RNA-seq analysis of WT cells with and without antimycin A (0.5 μg/ml) treatment. The total number of genes in each functional category is displayed in parentheses, and the percent of all differentially expressed genes is indicated. BP: biological process; CC: cell component; MF: molecular function. (**C**) Heatmap of the expression of genes encoding components of ETC in the WT versus WT with antimycin A treatment. Samples are clustered according to expression similarity and the differences in transcript levels were significant ($P < 0.05$). The corresponding genes are listed in Table S1.

Figure 2

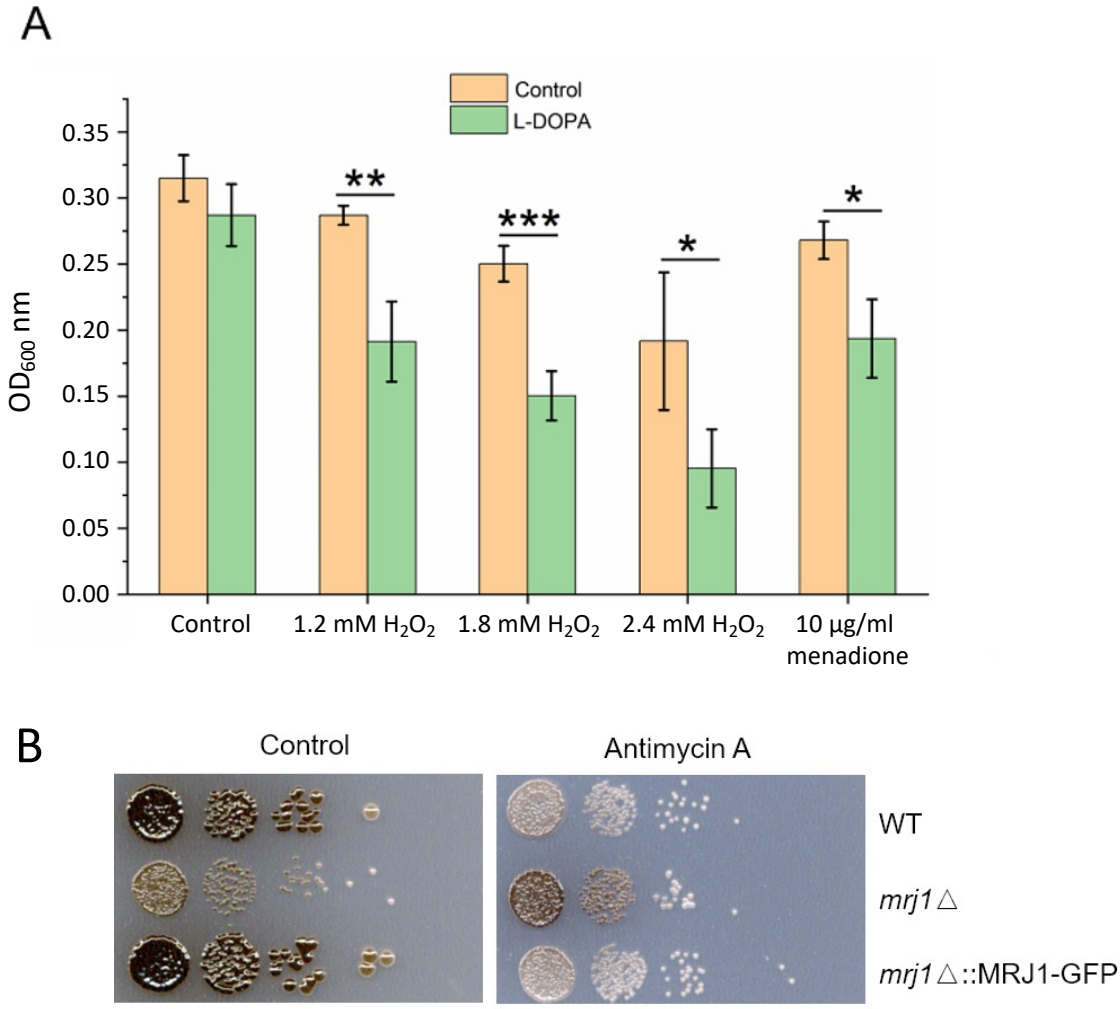

FIG 2 Growth and melanin formation are influenced by L-DOPA, oxidative stress, and the mitochondrial regulator Mrj1. (**A**) The growth of WT cells was tested in liquid medium with and without 0.7 mM L-DOPA in the presence of hydrogen peroxide (H_2O_2) or menadione at the indicated concentrations for 18 h at 30° C and 180 rpm in the dark. The assays were performed using 96-well microplates with each well containing a final volume of 200 μl. The initial cell density was set at 1×10^5 cells/ml. Mean values of three biological replicates are shown ± standard deviation (SD). Significant differences were determined by t tests and are indicated by * ($P < 0.05$), ** ($P < 0.01$), or *** ($P < 0.005$). (**B**) Spot assays of WT, *mrj1Δ* and *mrj1Δ*::*MRJ1-GFP* strains showing that the absence of *MRJ1* rescues melanin formation on L-DOPA plates in the presence of antimycin A (0.5 μg/ml). Plates were incubated for 72 h at 30° C in the dark.

Figure 3

A

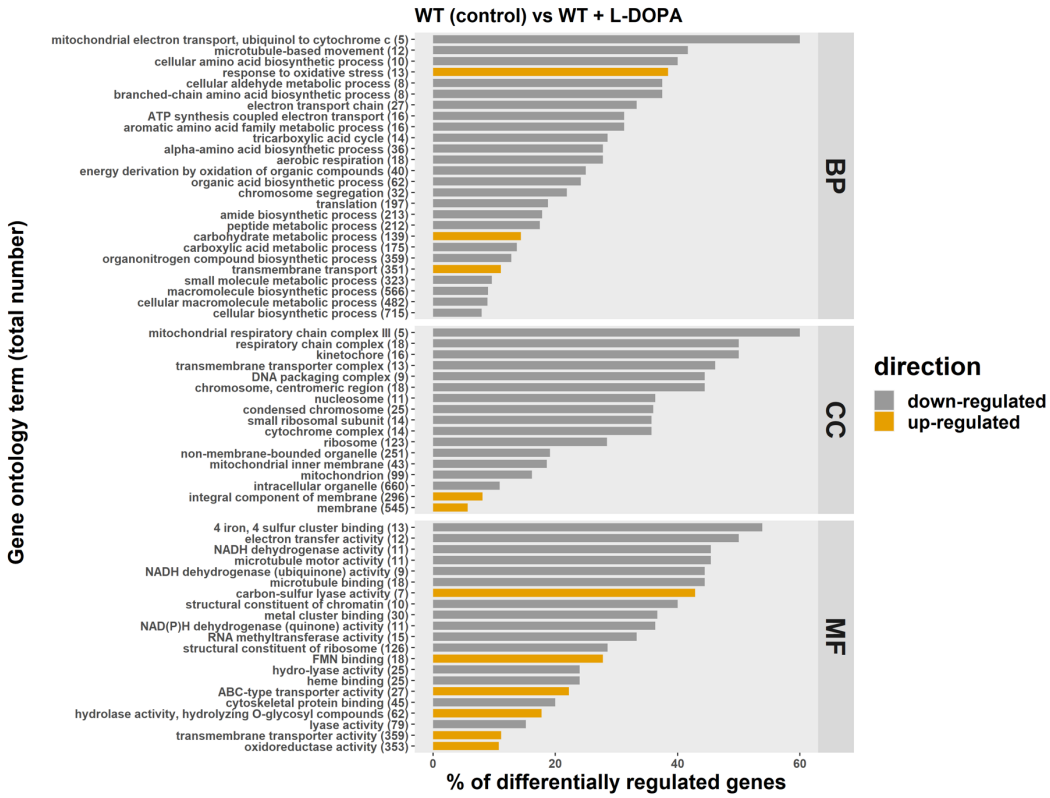
WT (control) vs WT + L-DOPA
Gene ontology term (total number)
mitochondrial electron transport, ubiquinol to cytochrome c (5)
microtubule-based movement (12)
cellular amino acid biosynthetic process (10)
response to oxidative stress (13)
cellular aldehyde metabolic process (8)
branched-chain amino acid biosynthetic process (8)
electron transport chain (27)
ATP synthesis coupled electron transport (16)
aromatic amino acid family metabolic process (16)
tricarboxylic acid cycle (14)
alpha-amino acid biosynthetic process (36)
aerobic respiration (18)
energy derivation by oxidation of organic compounds (40)
organic acid biosynthetic process (62)
chromosome segregation (32)
translation (197)
amide biosynthetic process (213)
peptide metabolic process (212)
carbohydrate metabolic process (139)
carboxylic acid metabolic process (175)
organonitrogen compound biosynthetic process (359)
transmembrane transport (351)
small molecule metabolic process (323)
macromolecule biosynthetic process (566)
cellular macromolecule metabolic process (482)
cellular biosynthetic process (715)
BP
mitochondrial respiratory chain complex III (5)
respiratory chain complex (18)
kinetochore (16)
transmembrane transporter complex (13)
DNA packaging complex (9)
chromosome, centromeric region (18)
nucleosome (11)
condensed chromosome (25)
small ribosomal subunit (14)
cytochrome complex (14)
ribosome (123)
non-membrane-bounded organelle (251)
mitochondrial inner membrane (43)
mitochondrion (99)
intracellular organelle (660)
integral component of membrane (296)
membrane (545)
CC
4 iron, 4 sulfur cluster binding (13)
electron transfer activity (12)
NADH dehydrogenase activity (11)
microtubule motor activity (11)
NADH dehydrogenase (ubiquinone) activity (9)
microtubule binding (18)
carbon-sulfur lyase activity (7)
structural constituent of chromatin (10)
metal cluster binding (30)
NAD(P)H dehydrogenase (quinone) activity (11)
RNA methyltransferase activity (15)
structural constituent of ribosome (126)
FMN binding (18)
hydro-lyase activity (25)
heme binding (25)
ABC-type transporter activity (27)
cytoskeletal protein binding (45)
hydrolase activity, hydrolyzing O-glycosyl compounds (62)
lyase activity (79)
transmembrane transporter activity (359)
oxidoreductase activity (353)
MF
0
20
40
60
% of differentially regulated genes
direction
down-regulated
up-regulated

B

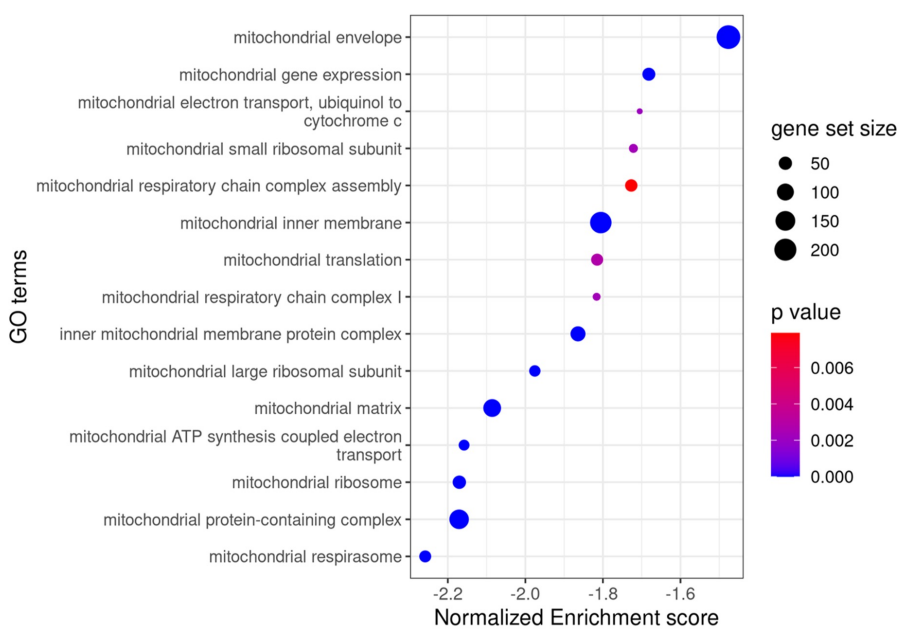
GO terms
mitochondrial envelope
mitochondrial gene expression
mitochondrial electron transport, ubiquinol to cytochrome c
mitochondrial small ribosomal subunit
mitochondrial respiratory chain complex assembly
mitochondrial inner membrane
mitochondrial translation
mitochondrial respiratory chain complex I
inner mitochondrial membrane protein complex
mitochondrial large ribosomal subunit
mitochondrial matrix
mitochondrial ATP synthesis coupled electron transport
mitochondrial ribosome
mitochondrial protein-containing complex
mitochondrial respirasome
-2.2
-2.0
-1.8
-1.6
Normalized Enrichment score
gene set size
50
100
150
200
p value
0.006
0.004
0.002
0.000

FIG 3 L-DOPA provokes down-regulation of mitochondrial functions. (**A**) Gene ontology (GO) terms for genes with differential transcriptions upon treatment with L-DOPA (0.7 mM). The total number of genes in each functional category is displayed in parentheses, and the percent of all differentially expressed genes is indicated on the x axis. BP: biological process; CC: cell component; MF: molecular function. (**B**) Gene Set Enrichment Analysis demonstrating negative enrichment for pathways directly involved in mitochondrial function. Significantly regulated pathways were determined using a 0.05 cut-off p-value and a false discovery rate of 0.25. The list of regulated genes for components of the ETC and iron-sulfur cluster biogenesis is presented in Table S2.

Figure 4

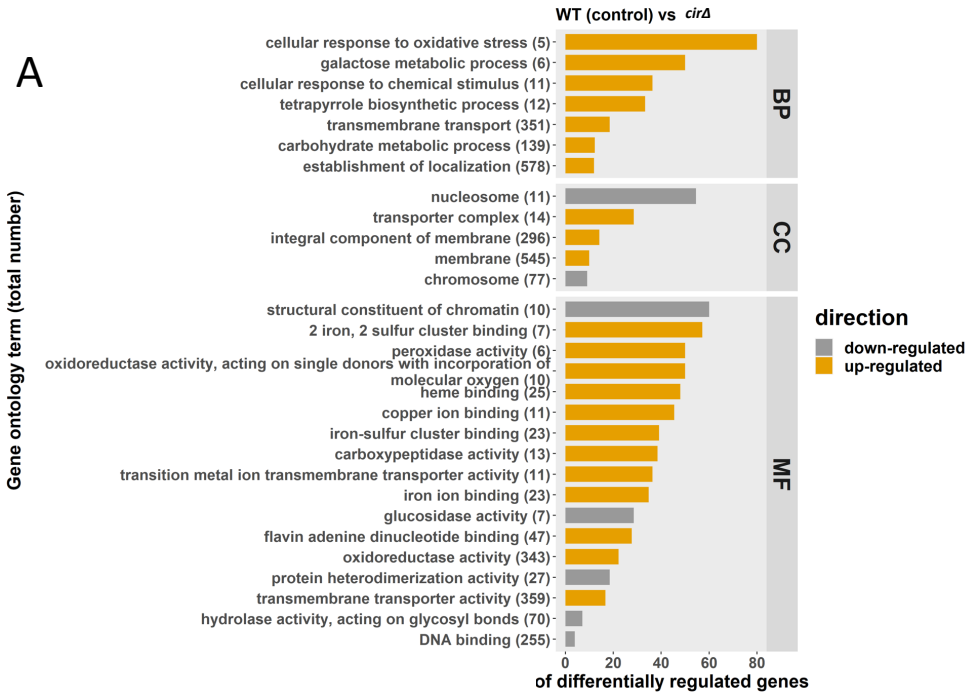

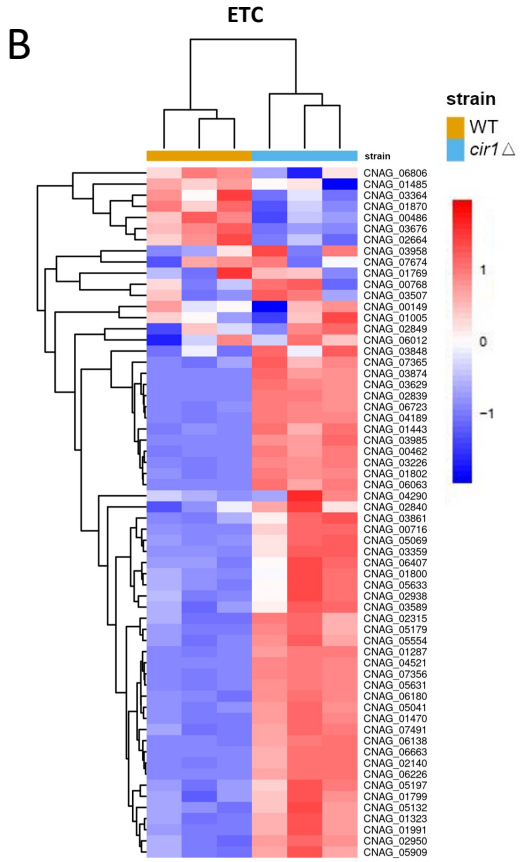

FIG 4 Loss of Cir1 results in up-regulation of mitochondrial functions. **(A)** Gene ontology (GO) terms for RNA-Seq analysis of the WT strain vs the *cir1Δ* mutant. The total number of genes in each functional category is displayed in parentheses, and the percent of all differentially expressed genes is indicated. BP: biological process; CC: cell component; MF: molecular function. (**B**) Heatmap of the expression of genes encoding components of electron transport chain (ETC) in the WT and *cir1Δ* mutant strains. The differences in transcript levels were significant ($P < 0.05$), and the corresponding genes are listed in Table S3.

Figure 5

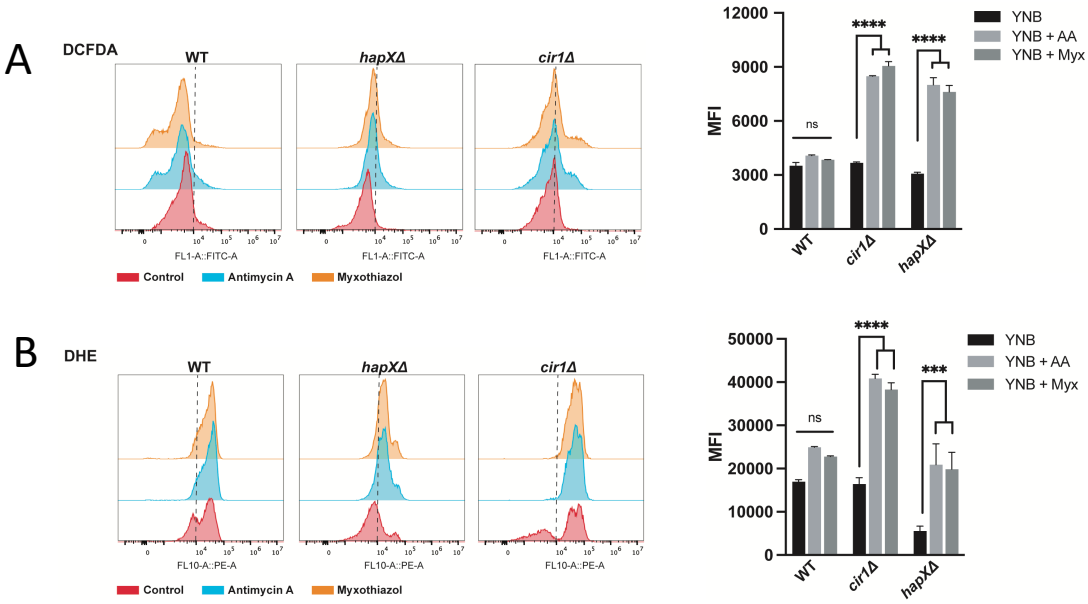

FIG 5. Loss of Cir1 or HapX results in accumulation of ROS in response to complex III inhibition. (**A**) Flow cytometry analysis of WT and mutant cells stained for 1 hour with 2′,7′-Dichlorofluorescein Diacetate (DCFDA, 16 µM) to detect ROS accumulation in response to exposure to antimycin A (AA, 50 µM) or myxothiazol (Myx, 7 µM) for 24 h at 30°C. (**B**) Flow cytometry analysis of WT and mutant cells stained with Dihydroethidium (DHE, 2.5 µg/ml) to detect ROS accumulation in response to ETC-III inhibitors as in (**A**). The data represent the mean fluorescent intensity (MFI, geometric means) from three biological replicates ± standard errors of the means. The statistical comparisons employed a two-way ANOVA test, followed by *post hoc* Šídák's or Tukey's multiple comparison tests (*, $P < 0.05$, **, $P < 0.01$ ***, $P < 0.001$; ****, $P < 0.0001$). ns: not significant. The gating strategy for the left panels is shown in Fig. S11.

Figure 6

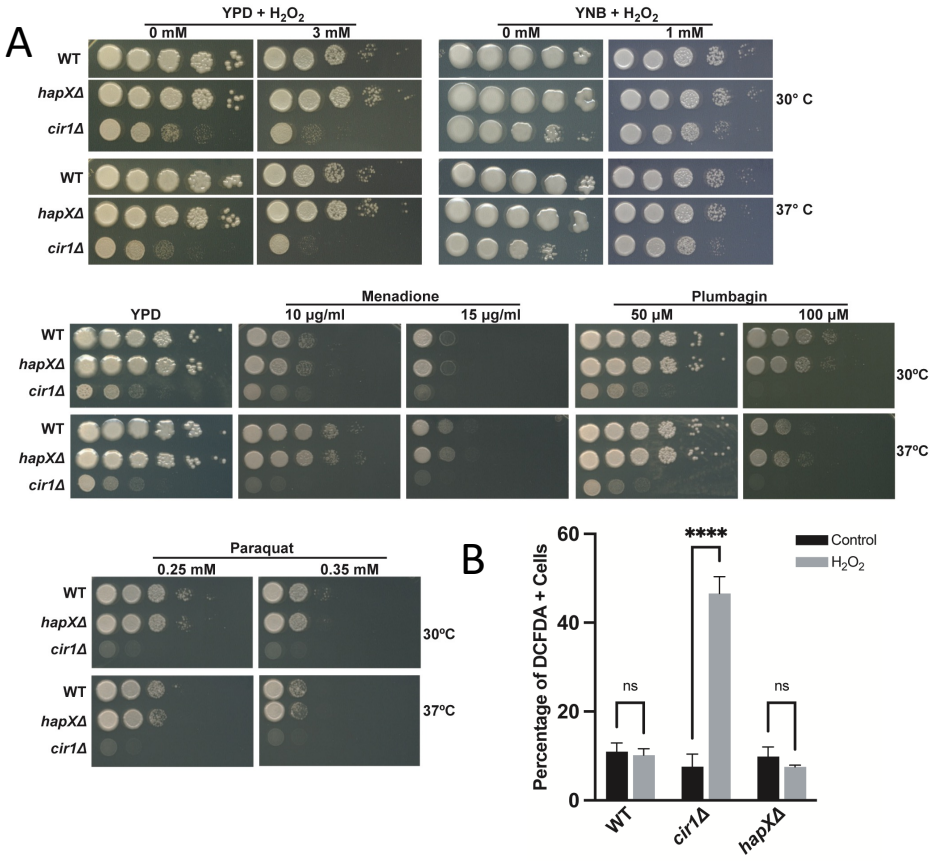

FIG 6 Loss of Cir1 but not HapX causes sensitivity to oxidative stress. **(**A) Spot assays of the WT strain and the *hapXΔ* or *cir1Δ* mutants on the indicated media were performed with 10-fold serial dilutions from an initial concentration of 2 x 10^7 cells per ml. Five microliters were spotted into solid YPD or YNB plates supplemented with different compounds and incubated at 30°C and 37°C for 2-3 days before being scanned. The media were supplemented at the indicated concentrations with the following compounds: hydrogen peroxide (H_2O_2), menadione, plumbagin, or paraquat. (**B**) Graph of the percentage of DCFDA positive cells upon exposure to H_2O_2 [5 mM] for 1 hour at 30°C for the WT strain and the *hapXΔ* and *cir1Δ* mutants as determined by flow cytometry using the gating strategy in Fig. S11. The data represent the average from at least three biological replicates ± standard errors of the means. Statistical comparisons employed a two-way ANOVA test, followed by *post hoc* Šídák's multiple comparison test (****, $P < 0.0001$). ns: not significant.

Figure 7

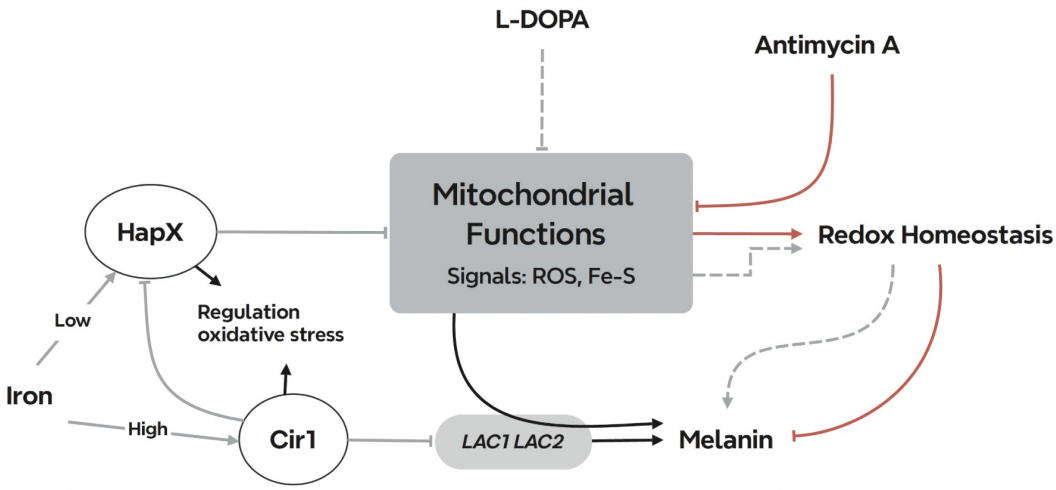

FIG 7. Summary model of the interplay between mitochondrial ETC function and the iron regulators that influence melanin formation in *C. neoformans*. Inhibitors of ETC complex III provoke ROS accumulation which inhibits melanin formation through an influence on laccase activity and/or localization. Cir1 directly represses transcription of the *LAC1* and *LAC2* genes encoding laccases, and loss of Cir1 may derepress the genes to a level sufficient partially restore melanin formation. Cir1 also represses the transcription of the *HAPX* gene (23, 31). HapX is a key regulator of iron-requiring functions in mitochondria, and loss of HapX derepresses genes for the response to oxidative stress. This de-repression may be sufficient to overcome ROS accumulation to partially restore melanin. Other signals including iron-sulfur clusters may be generated by ETC inhibition to include the activities of the iron regulators and the laccases.